Simulation of Resonant Magnetic Field Penetration Dynamics with the TEAR Code

N.V. Ivanov, A.M. Kakurin

National Research Centre «Kurchatov Institute», Moscow, Russia

It is well known that externally applied Resonant Magnetic Perturbation (RMP) can generate magnetic islands and consequently penetrate through the resonant magnetic surface [1-5]. This effect attracts considerable attention in the experimental and theoretical magnetic fusion research because RMP loops are often used in the present tokamak experiments and are designed for future tokamaks including ITER.

The process of RMP penetration is usually analyzed under assumption that the mode rotation is coupled with the rotation of resonant plasma layer. This well known no-slip constraint has been introduced in [2]. Besides that the poloidal rotation of plasma is omitted in some papers on the RMP penetration. However, there are some evidences [6] that the no-slip approximation is not valid for sufficiently small magnetic islands because the island velocity can deviate from plasma velocity due to finite plasma resistivity and consequent magnetic reconnections. The plasma poloidal rotation can also play some role in the field penetration process despite the high value of poloidal viscosity. This is expected because the ratio between viscous torque and plasma viscosity is much less for poloidal direction than for toroidal one for similar rotation velocities.

Results of TEAR code simulation and analysis of the RMP penetration are presented. The effects of the magnetic island and plasma velocity decoupling and of the plasma poloidal rotation on the RMP penetration are the main subjects of this paper. The TEAR code [6-8] is based on two-fluid MHD approximation that gives coupled diffusion-type equations for the magnetic flux perturbation and for the plasma rotation velocities in toroidal and poloidal directions. The radial distribution of the magnetic flux perturbation is calculated with account of an externally applied RMP and RMP component generated by eddy current in the resistive vacuum vessel. Variations of magnetic island width and rotation velocity under RMP due to finite plasma resistivity are taken into account [6]. An externally applied magnetic flux can diffuse across the plasma in the so-called magnetic-reconnection layer where the ideal-plasma assumption breaks down. The flux diffusion results in rearrangement of magnetic field topology that depends on the angular position of RMP with respect to the mode.

Integration of the equation of motion over the resonant layer gives equations for the toroidal and poloidal rotation velocities of the resonant layer depending on toroidal and poloidal moments of inertia of the plasma resonant layer, electromagnetic and viscous torques. Viscous friction torques are calculated under the assumption that poloidal viscosity is two orders of magnitude higher than toroidal one.

Simulation results of the RMP penetration dynamics are presented with the view of TEAR code validation against COMPASS-C tokamak experimental data [1]. We consider typical Ohmic COMPASS-C discharge in which application of helical (2, l) RMP causes mode penetration. The experimental dynamics of this process is shown in *Figure 2* in Ref. [1]. In this figure, one can see that locked mode signal indicates the RMP penetration as a sudden growth of a large stationary mode. Available COMPASS-C plasma characteristics are used for the modelling. We use values of resistive time τ_R = 45 ms, toroidal viscous time τ_ν = 22 ms, intrinsic value of the mode natural frequency $\Omega_{\mathrm{nat}\,0}/2\pi = \left(mV_{\theta 0}/r_{\mathrm{S}} - nV_{\varphi 0}/R - \omega^*\right)\Big|_{r_{\mathrm{S}}}/2\pi = -14\ \mathrm{kHz}$, initial toroidal, $\omega_{\varphi 0}/2\pi = 3\ \mathrm{kHz}$, and poloidal, $\omega_{\theta 0} = 0$, rotation frequencies and frequency of electron diamagnetic drift $\omega^*/2\pi = 11\ \mathrm{kHz}$.

The results of COMPASS-C experiment simulations are shown in FIG.1 and FIG.2. The simulations taking into account the effect of magnetic island and plasma velocity deviations are shown in the left columns (*a*) of these figures. The results of simulations fulfilled under the no-slip approximation are shown for comparison in the right columns (*b*). The RMP penetration process appearing as a change of natural frequency to $\Omega_{\mathrm{nat}} = 0$ value and a quick rise of the non-rotating island is in good agreement with the experimental data. In FIG.1(*a*) and FIG.2(*a*), the penetration is preceded by formation of stationary non-rotating small magnetic island in rotating plasma (see also [9]). In addition, the simulation shows a spin-up event similar to the experiment after the RMP is switched off. The induced island first unlocks from the RMP field and then decays away on a resistive time-scale.

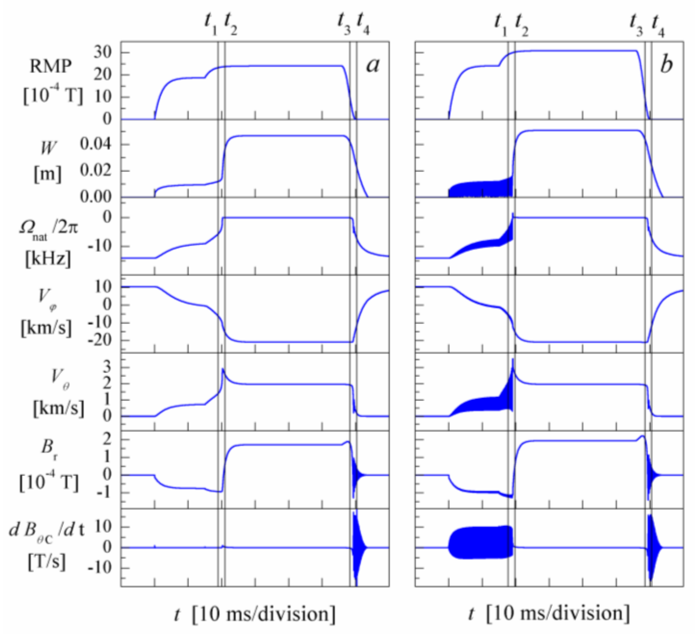

FIG.1. Simulation results of the RMP penetration dynamics in the COMPASS-C tokamak: radial component of RMP, magnetic island width (W), instantaneous value of mode natural frequency (Ω_{nat}), toroidal (V_φ) and poloidal (V_θ) velocities of resonant plasma layer, radial component of the mode magnetic field (B_r) at plasma boundary, and poloidal field time-derivative ($dB_{\theta C}/dt$)

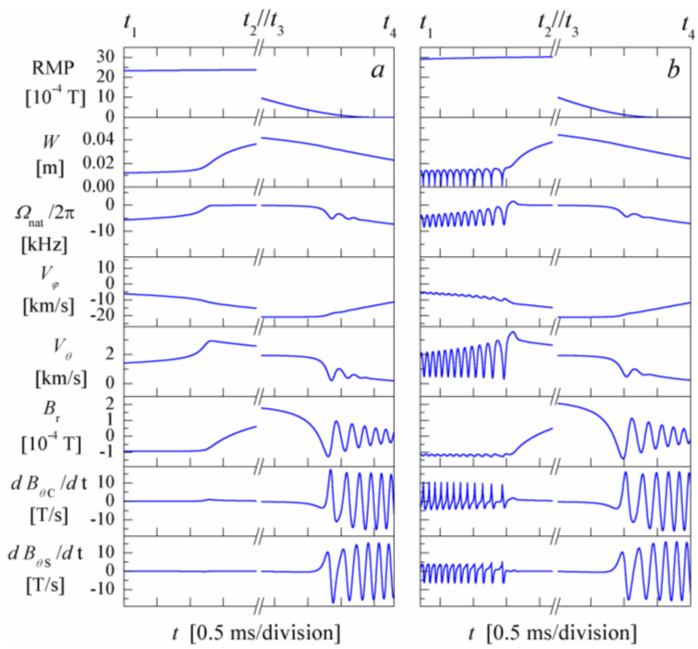

FIG.2. Simulation results of the RMP penetration dynamics in the COMPASS-C tokamak in the time intervals shown with vertical straight lines in FIG.1

Like in the experiment (see *Figure 2* in Ref. [1]), calculations made under the assumption that magnetic island and plasma velocity deviations are not forbidden (see left panels in FIG.1 and FIG.2) do not give oscillations of the $dB_{\theta C}/dt$ waveform before start of the RMP penetration process. On the contrary, the calculations under the no-slip approximation shown in the right (b) panels in FIG.1 and FIG.2 give frequent oscillations of the magnetic island width, W, before start of the field penetration process. These W oscillations are followed by a significant rise of the $dB_{\theta C}/dt$ oscillation amplitude. One should note that these $dB_{\theta C}/dt$ oscillations are not observed in the experiment.

Similar to the experiment, one can see in FIG.1 and FIG.2 a change of the plasma toroidal velocity to $V_\varphi = -21$ km/s value in the process of RMP penetration. According to calculations with no plasma poloidal rotation, the toroidal velocity turns to $V_\varphi = -38.4$ km/s after the RMP penetration. This value differs from the experimental one.

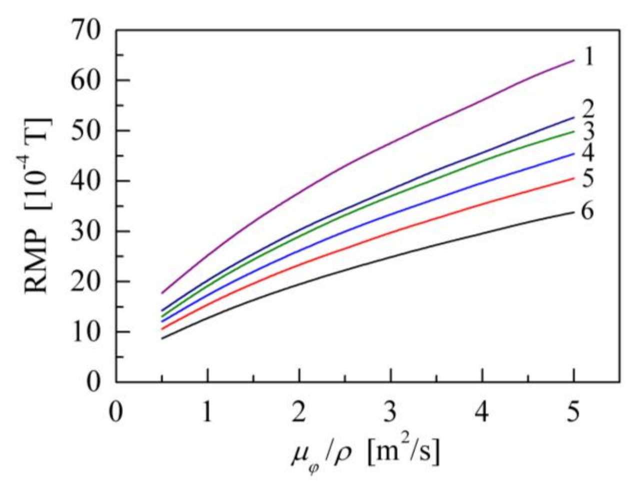

FIG.3. Dependences of RMP penetration threshold values on toroidal plasma viscosity in conditions: no-slip approximation and no poloidal rotation (1); account of island and plasma velocity deviations, no poloidal rotation (2); no-slip approximation, account of poloidal rotation (3); full model (island and plasma velocity deviations, account of poloidal rotation) $\mu_\theta/\mu_\varphi = 200$ (4), $\mu_\theta/\mu_\varphi = 100$ (5), $\mu_\theta/\mu_\varphi = 50$ (6)

The comparison of the left (a) and right (b) panels in Fig.1 and FIG.2 shows that the RMP penetration threshold is lower if the no-slip constraint is omitted and deviations of magnetic island velocity with respect to plasma are taken into account. Besides that the account of the plasma poloidal rotation also decreases the value of RMP penetration threshold. These results are also presented in FIG.3. In addition, one can see that the threshold value of the RMP penetration increases with the rise of the toroidal and poloidal plasma viscosity. The curves in FIG.3 are proportional to $(\mu_\varphi/\rho)^{7/12}$ that is similar to the prediction in [10].

Summary

In this paper the main attention was paid to dynamics of RMP penetration. The results of simulations with account of mode and plasma decoupling and plasma poloidal rotation are consistent with experimental data. The deviations between rotation velocities of magnetic island and plasma due to final plasma resistivity as well as plasma poloidal rotation reduce the RMP penetration threshold.

[1] Hender T.C., et al. Nucl. Fusion **32** (1992) 2091.

[2] Fitzpatrick R. Nucl. Fusion **33** (1993) 1049.

[3] Kikuchi Y., et al. Plasma Phys. Control. Fusion **48** (2006) 169.

[4] Yu Q., et al. Nucl. Fusion **48** (2008) 024007.

[5] Wang N., et al. Nucl. Fusion **54** (2014) 064014.

[6] Eliseev L.G. et al. Physics of Plasmas **22** (2015) 052504.

[7] Ivanov N., et al. 24th IAEA FEC (2012) TH/P3-22,
PAS&T/TF 36, v. 2, p. 55 (2013), see http://vant.iterru.ru/vant_2013_2/6.pdf.

[8] N.V. Ivanov and A.M. Kakurin. Physics of Plasmas **21** (2014) 102502.

[9] N.V. Ivanov and A.M. Kakurin, in 38th EPS Conference on Plasma Physics (2011), P2.080,
see http://ocs.ciemat.es/EPS2011PAP/pdf/P2.080.pdf;
PAS&T/TF (2012) 1, p. 64, see http://vant.iterru.ru/engvant_2012_1/6.pdf.

[10] R.J. Buttery, et al. Nucl. Fusion **39** (1999) 1827.